Broadband Ground-Plane Cloak

R. Liu,[1]* C. Ji,[2]* J. J. Mock,[1] J. Y. Chin,[3] T. J. Cui,[3]† D. R. Smith[1]†

The possibility of cloaking an object from detection by electromagnetic waves has recently become a topic of considerable interest. The design of a cloak uses transformation optics, in which a conformal coordinate transformation is applied to Maxwell's equations to obtain a spatially distributed set of constitutive parameters that define the cloak. Here, we present an experimental realization of a cloak design that conceals a perturbation on a flat conducting plane, under which an object can be hidden. To match the complex spatial distribution of the required constitutive parameters, we constructed a metamaterial consisting of thousands of elements, the geometry of each element determined by an automated design process. The ground-plane cloak can be realized with the use of nonresonant metamaterial elements, resulting in a structure having a broad operational bandwidth (covering the range of 13 to 16 gigahertz in our experiment) and exhibiting extremely low loss. Our experimental results indicate that this type of cloak should scale well toward optical wavelengths.

Transformation optics is a method for the conceptual design of complex electromagnetic media, offering opportunities for the control of electromagnetic waves (*1*, *2*). A wide variety of conventional devices can be designed by the transformation optical approach, including beam shifters (*3*), beam bends (*4*), beam splitters (*3*), focusing and collimating lenses (*5*), and structures that concentrate electromagnetic waves (*6*, *7*). Whereas all of these devices have properties that are unique to the class of transformation optical structures, one of the most compelling and unprecedented concepts to emerge has been that of a medium that can conceal objects from detection by electromagnetic waves. The prospect of electromagnetic cloaking has proven a tantalizing goal, with numerous concepts currently under investigation (*1*, *2*, *8*–*14*).

In the transformation optical approach, one imagines warping space so as to control the trajectories of light in a desired manner. As an example of this approach, a cloak can be designed by performing a coordinate transformation that squeezes the space from within a sphere to within a shell having the same outer radius. Waves do not interact with or scatter from the core because it is simply not part of the transformed space. The form invariance of Maxwell's equations implies that the coordinate transformation can instead be applied to the permittivity and permeability tensors, yielding the prescription for a medium that will accomplish the desired functionality. The resulting medium is highly complex, being anisotropic and with spatial gradients in the components of the permittivity and permeability tensors.

Such complicated gradient-index media are difficult to create with conventional materials but are much easier to build with artificially structured metamaterials, in which spatial variations of the material parameters can be achieved by modifying the geometry and placement of the constituent element. Even so, the large number of elements required in an arbitrary cloak medium can represent a substantial computational burden resulting in long design cycles. To address this time-consuming design step, we have developed a systematic algorithm that is applied once the spatial distribution of the constitutive parameters has been determined by the transformation. Previously, metamaterial structures requiring spatial gradients have been obtained by designing one unit cell at a time until a library of unique metamaterial elements, whose constitutive parameters span the range required by the transformation optical design, is generated. In contrast, the algorithm we use (*15*) requires only a comparatively small number of simulations of the metamaterial element, relying on a regression scheme to generate the functional dependence of the constitutive parameters on the unit cell geometry. The reduced number of simulations vastly speeds the metamaterial cloak-design process and makes the design of complex media possible.

The specification of a ground-plane cloak can be determined in the manner described in (*16*). If waves are restricted to a single plane of incidence, with the polarization of the waves being transverse electric (electric field perpendicular to the plane of incidence or parallel to the ground plane), then the cloak parameters need only be determined across a two-dimensional (2D) plane. The domain of the problem is thus a 2D space, filled with a uniform dielectric with refractive index value n_b and bounded by a conducting sheet. A family of coordinate transformations that will map a given nonplanar conducting surface to a planar surface can be found; however, such transformations generally lead to an anisotropic medium with values of n_x and n_y that vary as a function of the spatial coordinate. Yet, given the restricted geometry, it is possible to find a coordinate map that minimizes the anisotropy in the permeability components. Defining an anisotropy factor as $\alpha = \max(n_x/n_y, n_y/n_x)$, transformations can be found for which α is near unity so that the isotropic refractive index value varies throughout the space. If n_b in the original space is sufficiently greater than unity, then the values for the refractive index of the cloaking structure are also greater than unity. Under these conditions, nonresonant metamaterial elements can be used, and the cloak can exhibit a broad frequency bandwidth (*15*).

In our particular design, we followed the optimization technique (*16*) for the transformation region, in which a quasi-conformal coordinate map is generated by minimizing the Modified-Liao functional (*17*, *18*) with slipping boundary conditions. The Jacobian matrix Λ that relates the physical and virtual systems is then computed numerically, from which the index distribution $n^2 = \frac{1}{\sqrt{|\Lambda^T \Lambda|}}$ of the cloak is found (here, T is the transpose of the Jacobian matrix). In our final design, $\alpha = 1.04$, which is treated as negligible (that is, we assume $n_x = n_y$).

A photograph of the fabricated sample, a color map indicating the transformed space, and the associated refractive index distribution are presented in Fig. 1. We assume that the entire cloak is embedded in a background material with refractive index $n_b = 1.331$. Under these assumptions, the transformation leads to refractive index values for the ground-plane cloak that range from $n = 1.08$ to 1.67 (values that can be achieved with the use of nonresonant metamaterial elements). On the right and left side of the sample in Fig. 1B, the refractive index distribution is uniform ($n_b = 1.331$), taking the value of the background material. Because the cloak is designed to be embedded in a higher dielectric region, we add an impedance matching layer (IML) that surrounds the entire structure, for which the index changes gradually and linearly from that of air to that of the background index (*15*). This step is taken to minimize reflection from the cloak surface when illuminated by a microwave beam within the scattering chamber, which exists in an $n = 1.0$ (air) environment. The procedure for designing the IML layer is described in (*15*). Because of the index gradient coupled with the cloak, we expect no amplitude scattering and only a slight offset of the wave reflected from the ground-plane structure due to the refractive index change. The effect should be similar to observing a mirror through a layer of glass; objects on the top of the mirror, within the cloaked region, remain hidden from detection (visualized by ray tracing in Fig. 1D). It is important to note that this type of cloaking phenomena is distinct from current scattering suppression technologies because it both eliminates backscattering and restores the reflected beam.

To implement the cloak defined by the index distribution presented in Fig. 1C and the associated background material and IML in Fig. 1B, the continuous theoretical constitutive parameter distribution must be approximated by a discrete number of metamaterial elements. In our design, the entire sample region is divided into 2-by-2–mm squares, requiring more than 10,000 elements, about 6000 of which are unique.

[1]Center for Metamaterials and Integrated Plasmonics, Department of Electrical and Computer Engineering, Duke University, Durham, NC 27708, USA. [2]Department of Statistical Science, Duke University, Durham, NC 27708, USA. [3]State Key Laboratory of Millimeter Waves, Southeast University, Nanjing 210096, China.

*These authors contributed equally to this work.
†To whom correspondence should be addressed. E-mail: tjcui@seu.edu.cn (T.J.C.); drsmith@duke.edu (D.R.S.)

The elements chosen to achieve the design are all variations of the structure shown in Fig. 2. By changing the dimension a, we are able to span the required index range of n = 1.08 to 1.67. After a well-established retrieval process, modified to include the effects of the finite unit cell size relative to the wavelength (*19*, *20*), the effective permittivity and permeability for a given element can be found via numerical simulation. A regression curve can then be made that relates the refractive index associated with a given element to the length a. Once a set of elements has been

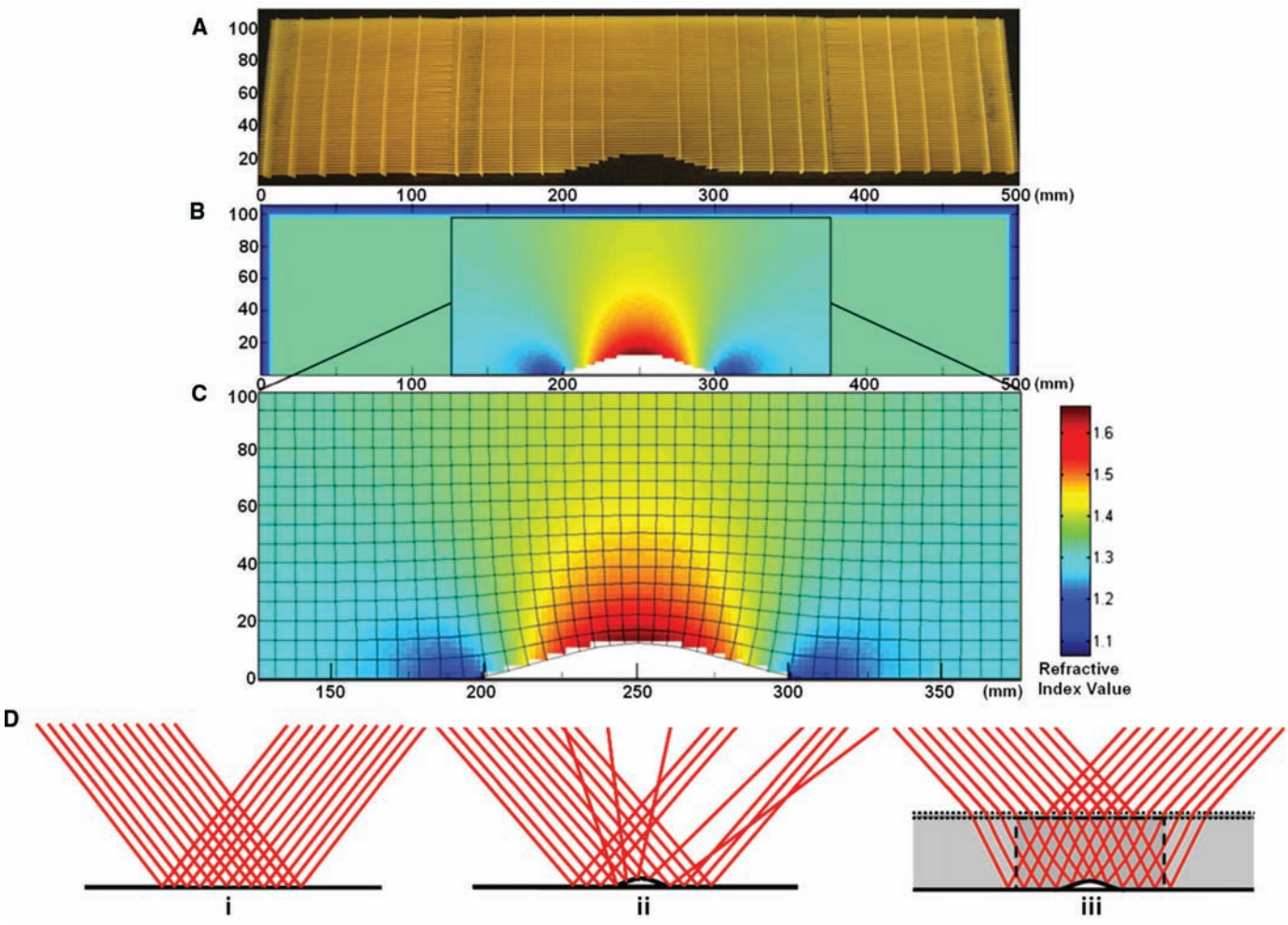

Fig. 1. The transformation optical design for the ground-plane cloak. The metamaterial cloak region is embedded in a uniform higher index background with gradients introduced at the edges to form impedance matching regions. (**A**) Photograph of the fabricated metamaterial sample. (**B**) Metamaterial refractive index distribution. The coordinate transformation region is shown within the box outlined in black. The surrounding material is the higher index embedding region and the IMLs. (**C**) Expanded view of the transformation optical region in which the mesh lines indicate the quasi-conformal mapping (lateral dimensions of the unit cells are ~3.5 times smaller). (**D**) Ray tracing of a beam incidents illuminating on (i) the ground, (ii) the perturbation, and (iii) the perturbation covered by a ground-plane cloak. The gray area and dashed lines in (iii) indicate the transformation region, embedded background material, and IML.

Fig. 2. The design of the nonresonant elements and the relation between the unit cell geometry and the effective index. The dimensions of the metamaterial unit cells are l = 2 mm, w_1 = 0.3 mm, w_2 = 0.2 mm, and a varying from 0 to 1.7 mm.

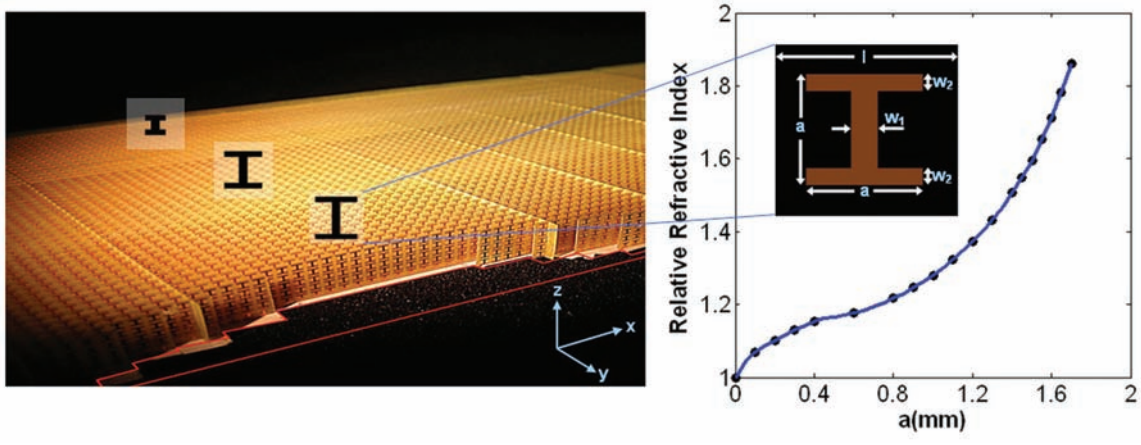

numerically simulated, all subsequent tasks in the cloak design—from the generation of the regression curve to the final layout of the elements in a mask for lithographic processing—are performed using a single Matlab program. The metamaterial elements we employ actually exhibit some degree of frequency dispersion in their constitutive parameters caused by their finite dimension with respect to the wavelength, as described in the supporting online material. In particular, the in-plane permeability and out-of-plane permittivity vary as a function of frequency such that the index stays approximately constant but the wave impedance varies considerably. Because the cell-to-cell change in impedance is minor, there is no reflection and no discernable disturbance in the cloak properties over the entire frequency range measured.

As with previous metamaterial designs implemented for microwave experiments, the final ground-plane cloak is fabricated on copper-clad printed circuit board with FR4 substrate (the substrate thickness is 0.2026 mm, with a dielectric constant of $3.85 + i0.02$). The completed sample is 500 by 106 mm with a height of 10 mm. The center region, 250 by 96 mm, corresponds to the transformed cloaking region, whereas the rest of the sample is used for dielectric embedding and impedance matching. The cloak transformation is specifically designed to compensate a perturbation introduced on the conducting surface that follows the curve $y = 12\cos^2[(x - 125)\pi/125]$ (units in millimeters).

To verify the predicted behavior of the ground-plane cloak design, we make use of a phase-sensitive, near-field microwave scanning system to map the electric field distribution inside a planar waveguide. The planar waveguide restricts the wave polarization to transverse electric. The details of the apparatus have been described previously (*21*). A large area field map of the scattering region, including the collimated incident and scattered beams, is shown in Fig. 3. The waves are launched into the chamber from a standard X-band coax-to-waveguide coupler and pass through a dielectric lens that produces a nearly collimated microwave beam. The beam is arbitrarily chosen to be incident on the ground plane at an angle of 40° with respect to the normal. A flat ground plane produces a near perfect reflection of the incident beam in Fig. 3A, whereas the presence of the perturbation produces considerable scattering, as shown in Fig. 3B (note the presence of the strongly scattered secondary beam). By covering the space surrounding the perturbation with the metamaterial cloaking structure, however, the reflected beam is restored, as if the ground plane were flat in Fig. 3C. The beam is slightly bent as it enters the cloaking region because of the refractive index change of the embedding material but is bent back upon exiting. The gradient-index IML introduced into the design minimizes reflections at the boundaries of the cloaking region.

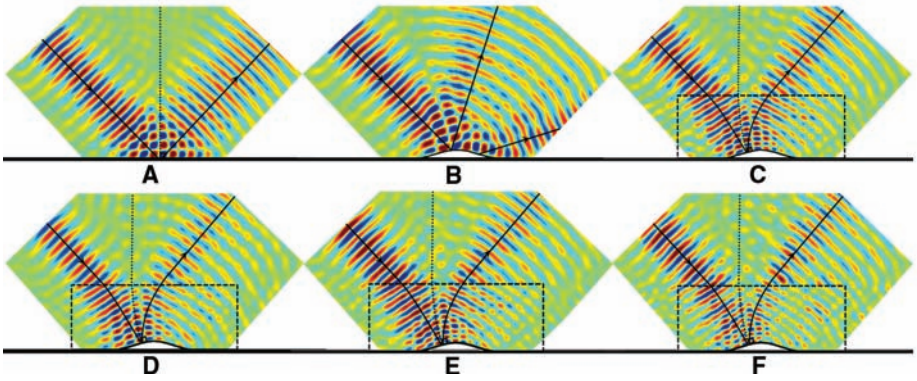

Fig. 3. Measured field mapping (E-field) of the ground, perturbation, and ground-plane cloaked perturbation. The rays display the wave propagation direction, and the dashed line indicates the normal of the ground in the case of free space and that of the ground-plane cloak in the case of the transformed space. (**A**) Collimated beam incident on the ground plane at 14 GHz. (**B**) Collimated beam incident on the perturbation at 14 GHz (control). (**C**) Collimated beam incident on the ground-plane cloaked perturbation at 14 GHz. (**D**) Collimated beam incident on the ground-plane cloaked perturbation at 13 GHz. (**E**) Collimated beam incident on the ground-plane cloaked perturbation at 15 GHz (**F**) Collimated beam incident on the ground-plane cloaked perturbation at 16 GHz.

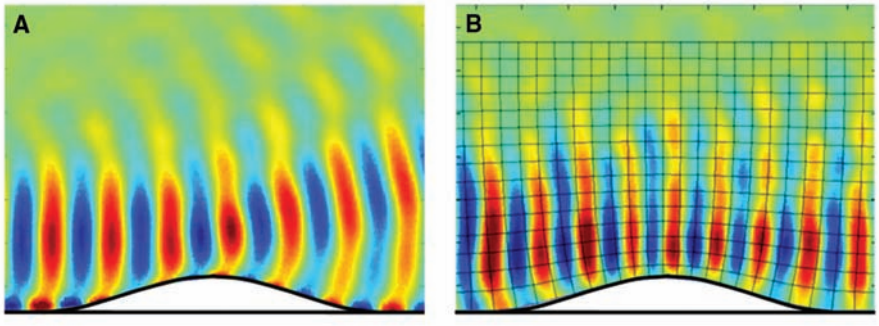

Fig. 4. 2D field mapping (E-field) of the perturbation and ground-plane cloaked perturbation, illuminated by the waves from the left side (**A**) perturbation and (**B**) ground-plane cloaked perturbation. The grid pattern indicates the quasi-conformal mapping of the transformation optics material parameters.

As the ground-plane cloak makes use of nonresonant elements, it is expected to exhibit a large frequency range of operation. The cloaking behavior was confirmed in our measurements from the range 13 to 16 GHz, though we expect the bandwidth to actually stretch to very low frequencies (<1 GHz) that cannot be verified experimentally because of limitations of the measurement apparatus and the beam-forming lens. We illustrate the broad bandwidth of the cloak with the field maps taken at 13 GHz in Fig. 3D, 15 GHz in Fig. 3E, and 16 GHz in Fig. 3F, which show similar cloaking behavior to the map taken at 14 GHz in Fig. 3C. The collimated beam at 16 GHz has begun to deteriorate because of multimode propagation in our 2D measurement chamber, which is also observed in the flat ground-plane control experiment at that frequency. However, on the basis of the predicted response of the broadband unit cells, we expect this cloak to function up to ~18 GHz.

To further visualize the performance of the ground-plane cloak, we illuminated the sample from the side (90° from the surface normal) with a narrow collimated beam. As the ground-plane cloaked perturbation should also be cloaked with the respect to an observer located on the ground, the wave, which should follow the metric as defined by the quasi-transformation map in Fig. 1, can be expected to detour around the perturbation and then return back to its original propagation direction. The field map for this case is shown in Fig. 4B, which corresponds with the predicted transformation extremely well (a low-resolution representation of the transformation grid is overlaid on the experimental data). For comparison, Fig. 4A shows a map of the field strongly scattered from the perturbation in the absence of the cloak.

The agreement between the measured field patterns for the ground-plane cloak and the theory (*16*) provides convincing evidence that metamaterials can indeed be used to construct such complex electromagnetic media. Although this cloak is not able to hide objects from detection that do not lie under the conducting curtain formed by the perturbation of the ground plane, its broadband and low-loss properties are compelling and offer a path toward realization of some forms of cloaking at frequencies approach-

ing the optical. By merging the nascent technique of transformation optics with traditional gradient-index optics, we have shown that more functional hybrid structures can be developed that enable us to access previously unseen electromagnetic behavior while mitigating some of the inherent limitations. Though transformation optical designs are highly complex, metamaterial implementations can be rapidly and efficiently achieved using the algorithms and approach described in this report.

References and Notes

1. J. B. Pendry, D. Schurig, D. R. Smith, *Science* **312**, 1780 (2006); published online 24 May 2006 (10.1126/science.1125907).
2. U. Leonhardt, *Science* **312**, 1777 (2006), published online 24 May 2006; 10.1126/science.1126493.
3. M. Rahm, S. A. Cummer, D. Schurig, J. B. Pendry, D. R. Smith, *Phys. Rev. Lett.* **100**, 063903 (2008).
4. M. Rahm *et al.*, *Opt. Express* **16**, 11555 (2008).
5. A. V. Kildishev, V. M. Shalaev, *Opt. Lett.* **33**, 43 (2008).
6. M. Rahm *et al.*, *Phot. Nano. Fund. Appl.* **6**, 87 (2008).
7. W. X. Jiang *et al.*, *Appl. Phys. Lett.* **92**, 264101 (2008).
8. Z. Ruan, M. Yan, C. W. Neff, M. Qiu, *Phys. Rev. Lett.* **99**, 113903 (2007).
9. A. Hendi, J. Henn, U. Leonhardt, *Phys. Rev. Lett.* **97**, 073902 (2006).
10. D. Schurig *et al.*, *Science* **314**, 977 (2006); published online 18 October 2006 (10.1126/science.1133628).
11. W. Cai, U. K. Chettiar, A. V. Kildishev, V. M. Shalaev, *Nat. Photon.* **1**, 224 (2007).
12. H. Chen, B. I. Wu, B. Zhang, J. A. Kong, *Phys. Rev. Lett.* **99**, 063903 (2007).
13. A. Alu, N. Engheta, *Phys. Rev. Lett.* **100**, 113901 (2008).
14. W. X. Jiang *et al.*, *Phys. Rev. E Stat. Nonlin. Soft Matter Phys.* **77**, 066607 (2008).
15. See the supporting material on *Science* Online.
16. J. Li, J. B. Pendry, *Phys. Rev. Lett.* **101**, 203901 (2008).
17. J. F. Thompson, B. K. Soni, N. P. Weatherill, *Handbook of Grid Generation* (CRC Press, Boca Raton, FL, 1999).
18. P. Knupp, S. Steinberg, *Fundamentals of Grid Generation* (CRC Press, Boca Raton, FL, 1994).
19. D. R. Smith, D. C. Vier, Th. Koschny, C. M. Soukoulis, *Phys. Rev. E Stat. Nonlin. Soft Matter Phys.* **71**, 036617 (2005).
20. R. Liu, T. J. Cui, D. Huang, B. Zhao, D. R. Smith, *Phys. Rev. E Stat. Nonlin. Soft Matter Phys.* **76**, 026606 (2007).
21. B. J. Justice *et al.*, *Opt. Express* **14**, 8694 (2006).

22. This work was supported by a gift from Raytheon Missile Systems (Tucson), and the rapid design approach was supported by a Multiple University Research Initiative supported by the Air Force Office of Scientific Research, contract no. FA9550-06-1-0279. T.J.C. acknowledges the support from InnovateHan Technology, National Science Foundation of China (60871016 and 60671015), National Basic Research Program (973) of China (2004CB719802), Natural Science Foundation of Jiangsu Province (BK2008031), and the 111 Project (111-2-05). We thank C. Harrison, N. Kundtz, and J. Allen for assistance for the experimental apparatus; A. Degiron for careful reading of the manuscript; Q. Cheng for the nonresonant element metamaterials technique development; and H. Schmitt, D. Barker (Raytheon Missile Systems), and M. West for helpful discussions.

Supporting Online Material

www.sciencemag.org/cgi/content/full/323/5912/366/DC1
SOM Text
Figs. S1 to S6
Movies S1 to S5

8 October 2008; accepted 5 December 2008
10.1126/science.1166949

Coherent Intrachain Energy Migration in a Conjugated Polymer at Room Temperature

Elisabetta Collini and Gregory D. Scholes*

The intermediate coupling regime for electronic energy transfer is of particular interest because excitation moves in space, as in a classical hopping mechanism, but quantum phase information is conserved. We conducted an ultrafast polarization experiment specifically designed to observe quantum coherent dynamics in this regime. Conjugated polymer samples with different chain conformations were examined as model multichromophoric systems. The data, recorded at room temperature, reveal coherent intrachain (but not interchain) electronic energy transfer. Our results suggest that quantum transport effects occur at room temperature when chemical donor-acceptor bonds help to correlate dephasing perturbations.

Numerous systems, such as natural photosynthetic proteins and artificial polymers, organize light-absorbing molecules (chromophores) to channel photon energy to create electronic or chemical gradients. The excitation energy from the absorbed light is either transferred through space or shared quantum mechanically among several chromophores (*1*). The interplay among these classical and quantum limits of electronic energy transfer (EET) dynamics is dictated by the way the chromophores communicate with each other via long-range Coulombic interactions, as well as by the strength of perturbations from the bath of fluctuating nuclear motions in the molecular architecture and surrounding external medium (*2*–*6*).

An elusive intermediate EET regime is of particular interest because the excitation moves in space—which is a deterministic, classical attribute—yet a preferred path can be adopted through wave function delocalization and associated interference effects, which introduce quantum characteristics to the dynamics (*7*). Together these attributes may in principle allow phase information to be transferred through space, with the electronic Hamiltonian of the entire system thereby steering EET. By learning how to observe the intermediate coupling case and thereafter to understand its properties, we could learn how to control excitation waves in a complex, multichromophoric system. Here, we present the results of an ultrafast spectroscopy experiment specifically designed to probe quantum coherent EET in the intermediate coupling case.

Rapid decoherence—the loss of memory of the initial electronic transition frequency distribution in an ensemble, caused by random fluctuations due to interaction of the system with its surroundings—is the primary reason for the scarcity of reports of coherent EET in complex condensed-phase systems. In the following, $|0\rangle$ designates the ground state, $|d\rangle$ is the donor, and $|a\rangle$ is the acceptor. According to theory, the evolution of the acceptor probability density in EET can be written as a product of forward ($|d\rangle$ to $|a\rangle$) and reverse propagations of the system [e.g., (*2*)], which allows us to describe how the competition between electronic interaction and decoherence determines the EET dynamics. In the strong coupling case, the electronic coupling period dominates over decoherence; therefore, forward and reverse donor-acceptor paths tend to be almost identical. Phase is preserved over each path, and a kind of standing wave connects the two states so that their evolution is intimately entangled in a quantum state. In the weak coupling case, the fluctuations of the electronic transition frequency of a chromophore occur faster than the characteristic time of the donor-acceptor coupling. Owing to the tremendous number of different possible trajectories of transition energy fluctuations that can occur, the forward and reverse donor-acceptor propagations differ, so that decoherence dominates and the excitation is localized on the donor or acceptor at any one time—but not on both simultaneously—and the EET dynamics follow classical rate laws.

The rate of EET is often measured by transient absorption spectroscopy, where an ultrafast laser pulse photoexcites the donor chromophores and a probe pulse monitors the probability that the excitation has been transferred to an acceptor as a function of pump-probe delay time *T*. When the donor and acceptor chromophores have similar excitation energies, they cannot be spectrally distinguished, so we instead record anisotropy as a function of *T*. This technique has been extensively exploited to study EET in various kinds of multichromophoric systems (*8*–*10*). The anisotropy decay is caused by any process that changes the orientation of the chromophores probed relative to those initially photoexcited. For instance, electronic excitation could pass between two segments that are oriented at an angle in space. Alternatively, an excited chromophore could physically

Department of Chemistry, Institute for Optical Sciences, and Center for Quantum Information and Quantum Control, University of Toronto, Toronto, Ontario M5S 3H6, Canada.

*To whom correspondence should be addressed. E-mail: gscholes@chem.utoronto.ca

Broadband Ground-Plane Cloak

R. Liu, C. Ji, J. J. Mock, J. Y. Chin, T. J. Cui and D. R. Smith

Science **323** (5912), 366-369.
DOI: 10.1126/science.1166949